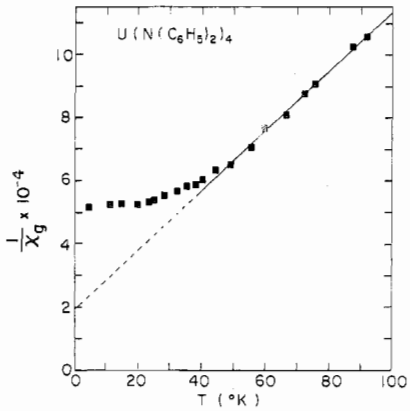

Figure 7. Inverse molar magnetic susceptibility of $U[N(C_6H_5)_2]_4$.

microcrystals, but no structure determination of these was possible.

We have found that uranium amides have a greater tendency to oligomerize than the d transition series amides. By proper choice of a bulky ligand we have been able to synthesize a monomer $U(N(C_6H_5)_2)_4$ in the solid state. The steric congestion is relieved in the oxygen-bridged product where one diphenylamide group is replaced, and the solid state structure is dimeric. In solution, $U(N(C_6H_5)_2)_4$ exhibits strong similarities to the other uranium amides. Once again the proton magnetic resonance and optical spectra indicate complexing with donating type solvents. In noncomplexing solvents, the tetrahedral structure is retained. It appears that with most of the uranium amides, the solid state structure is not necessarily the same as the solution species.

Acknowledgment. This work was done with support from the U.S. Energy Research and Development Administration.

Registry No. $U(dpa)_4$, 61900-16-1; $(UO(dpa)_3LiOEt_2)_2$, 62005-87-2; $U(NEt_2)_4$, 40678-59-9.

Supplementary Material Available: Formulas used in data reduction and listings of the structure factors (35 pages). Ordering information is given in any current masthead page.

References and Notes

(1) R. G. Jones, G. Karmas, G. A. Martin, Jr., and H. Gilman, *J. Am. Chem. Soc.*, **78**, 4285 (1956).
(2) K. W. Bagnall and E. Yanir, *J. Inorg. Nucl. Chem.*, **36**, 777 (1974).
(3) J. D. Jamerson and J. Takats, *J. Organomet. Chem.*, **78**, C23 (1974).
(4) J. G. Reynolds, A. Zalkin, D. H. Templeton, N. Edelstein, and L. K Templeton, *Inorg. Chem.*, **15**, 2498 (1976).
(5) J. G. Reynolds, A. Zalkin, D. H. Templeton, and N. M. Edelstein, *Inorg. Chem.*, **16**, 599 (1977).
(6) Professor J. Takats of University of Alberta, Alberta, Canada has informed us that he has also synthesized this compound and has characterized it by its proton magnetic resonance spectrum and mass spectrum.
(7) H. St. Räde, *J. Phys. Chem.*, **77**, 424 (1973).
(8) M. H. Chisholm, F. A. Cotton, M. Extine, and B. R. Stults, *J. Am. Chem. Soc.*, **98**, 4477 (1976).
(9) D. C. Bradley, M. B. Hursthouse, and C. W. Ewing, *Chem. Commun.*, 411 (1971).
(10) C. Heath and M. B. Hursthouse, *Chem. Commun.*, 143 (1971).
(11) D. C. Bradley, M. H. Chisholm, C. E. Heath, and M. B. Hursthouse, *Chem. Commun.*, 1261 (1969).
(12) F. A. Cotton, B. R. Stults, J. M. Troup, M. H. Chisholm, and M. Extine, *J. Am. Chem. Soc.*, **97**, 1242 (1975).
(13) M. H. Chisholm and W. Ruchert, *J. Am. Chem. Soc.*, **96**, 1249 (1974).
(14) O. Kennard, "International Tables for X-ray Crystallography", Vol. III, Kynoch Press, Birmingham, England, 1962, Table 4.2.4.
(15) D. C. Bradley, *MTP Int. Rev. Sci.: Inorg. Chem., Ser. One*, **5**, 82 (1972).
(16) D. C. Bradley and M. H. Chisholm, *Acc. Chem. Res.*, **9**, 272 (1976).
(17) D. C. Bradley and I. M. Thomas, *J. Chem. Soc.*, 3857 (1960).
(18) D. C. Bradley and I. M. Thomas, *Can. J. Chem.*, **40**, 449 (1962).
(19) D. C. Bradley and I. M. Thomas, *Can. J. Chem.*, **40**, 1355 (1962).
(20) The ^1H NMR results of Professor Takats are in good agreement with our work.
(21) D. R. Eaton and W. D. Phillips, *Adv. Magn. Reson.*, **1**, 103 (1965).
(22) K. R. Lea, J. J. M. Leash, and W. P. Wolf, *J. Phys. Chem. Solids*, **23**, 1381 (1962).
(23) C. A. Hutchison, Jr., and G. A. Candela, *J. Chem. Phys.*, **27**, 707 (1957).

Contribution from the Department of the Geophysical Sciences, The University of Chicago, Chicago, Illinois 60637

Mitridatite, $Ca_6(H_2O)_6[Fe^{III}_9O_6(PO_4)_9]\cdot 3H_2O$. A Noteworthy Octahedral Sheet Structure

PAUL BRIAN MOORE* and TAKAHARU ARAKI

Received November 23, 1976 AIC608439

A natural single crystal of mitridatite, asymmetric unit $Ca_6(H_2O)_6[Fe^{III}_9O_6(PO_4)_9]\cdot 3H_2O$, was studied in detail by three-dimensional x-ray diffractometry. The compound is monoclinic and possesses space group Aa, $Z = 4$, $a = 17.553$ (2), $b = 19.354$ (3), $c = 11.248$ (2) Å, $\beta = 95.84$ (1)°. $R = 0.068$ ($R_w = 0.082$) for 5547 independent reflections. X-ray diffraction data to $(\sin\theta)/\lambda = 0.70$ (Mo $K\alpha_1$ radiation) were collected on a Picker FACS-1 automated diffractometer and the structure was solved by Patterson, Fourier, chemical-intuitive and least-squares refinement techniques. The underlying principle is a compact sheet of composition $[Fe^{III}_9O_6(PO_4)_9]^{12-}$ oriented parallel to the {100} plane and located at $x \sim {}^1/_4$ and ${}^3/_4$. It has trigonal pseudosymmetry $a = 11.25$ Å (=c of mitridatite cell) and two-sided plane group $p31m$ and is locally isomorphic to a sheet of composition $[Na_9F_6(SO_4)_9]^{15-}$ found in the crystal structure of schairerite, $Na_{21}F_6Cl(SO_4)_7$, $Z = 3$. The sheet is built of octahedral Fe^{3+}–O edge-sharing nonamers decorated above, below, and in the plane by the PO_4 tetrahedra.

Introduction

Mitridatite, a basic calcium ferric phosphate, is a widely distributed although ill-defined phase in low-temperature sedimentary environments. Earlier described as crusts and nodules from the oolitic sedimentary iron ore deposits in the Kerch and Taman peninsulas, southern Russia,[1-3] it also occurs as a common product of weathering of exposed primary iron phosphates in pegmatites and other granitic rocks,[4] and in ferruginous soils, marls, and sandstones which have been impregnated with organic remains. Such field evidence suggests that the phase is quite stable and possibly one of the most important ferric phosphates formed under rather neutral conditions and ambient temperatures as prevail on the surface of the Earth. Its typical appearance as dull-green to brownish-green earthy stains and films are hardly good distinguishing characters and only the trained eye lifts it out of its undeserved obscurity in natural systems.

Mitridatite has posed some difficult problems for the investigator. Satisfactory single crystals are a great rarity and variable composition of cryptocrystalline masses is typical. The

Table I. Experimental Details of Mitridatite

(A) Crystal Cell Data	
a, Å	17.553 (2)
b, Å	19.354 (3)
c, Å	11.248 (2)
β, deg	95.84 (1)
Space group	Aa
Z	4
Formula	$Ca_6(H_2O)_6[Fe^{III}_9O_6(PO_4)_9]\cdot 3H_2O$
ρ(calcd), g cm^{-3}	3.249
Specific gravity[4]	3.24
μ, cm^{-1}	
(B) Intensity Measurements	
Crystal size, mm	0.046(||a), 0.21(||b), 0.22(||c)
Crystal orientation	ϕ axis = [100]
Max (sin θ)/λ	0.70
Scan speed, deg per min	2.0
Base scan width	2.5
Background counts	Stationary, 20 s at beginning and end of scan
Radiation	Mo Kα_1 (λ 0.7926 Å), graphite monochromator
Independent F_o	5547
(C) Refinement of the Structure	
R	0.068
R_w	0.082
Scale factor	0.900 (3)
Goodness of fit	1.00 (readjusted)
Coefficient of extinction	0.39 (11) × 10^{-7}

senior investigator searched for one decade and accumulated thousands of specimens from hundreds of pegmatites distributed over six continents until the quest was rewarded. A further three years' effort was devoted to unravelling its crystal structure, which proved to be an arrangement of unusual but elegant complexity. We earlier announced preliminary results of this study[5] and now proceed with a detailed crystal-chemical account of this fascinating phase.

Experimental Section

Preliminary crystal cell data on mitridatite, including the contents, unit cell, and space group, constituted the first formal study of the phase.[4] In that study, the possible compositions $8[Ca_3Fe^{III}_4(OH)_6(PO_4)_4\cdot 3H_2O]$ or $4[Ca_6Fe^{III}_9(OH)_{15}(PO_4)_8\cdot 9H_2O]$ were proposed. Unusual problems were encountered including persistent twinning by rotation of $\pm\pi/3$ radians on {100}, and a pronounced pseudo-trigonal subcell with b(sub) = $b/3$ and $3^{1/2}b$(sub) ≈ c. The crystal selected was described in the earlier study[4] and originated from the White Elephant pegmatite, near Custer, S.D. Preliminary precession and Weissenberg photographs on the red-black crystal showed no evidence of twinning and revealed uniform spot shape and low mosaic spread.

Table I lists the experimental details in this study. Utilizing a Picker FACS-1 automated four-circle diffractometer, least-squares refinement of 16 high-angle reflections led to the cell parameters and estimated standard deviations in Table I. Owing to its thin tabular habit, the crystal was carefully measured and the raw intensities were corrected for absorption anisotropy, applying 6 × 6 × 6 grid points and the Gaussian integral method for path lengths.[6] Estimated errors of the intensities (σ_I) were calculated according to an earlier published procedure.[7] For the $|F_o|$ data set, the symmetry-equivalent ($0kl$) and ($0k\bar{l}$) structure factor pairs and their errors were averaged.

Structure Determination and Refinement. Programs used in determining the structure were listed earlier.[7] The analysis of the structure proved to be a miserable problem. Three-dimensional Patterson synthesis, $P(uvw)$, revealed a map exhibiting pronounced substructure with b(sub) = $b/3$ and $3^{1/2}b$(sub) ≈ c. In addition, the vector densities of the substructure approximated trigonal symmetry, the subcell mentioned above being the orthohexagonal unit. Strong densities occur at the u = 0 and $^1/_2$ levels and we interpreted these as Fe atoms in special positions along the twofold rotor and in general positions at x = $^1/_4$, $^3/_4$ in space group $A2/a$. At this stage, we suspected local isomorphism with the crandallite, $Ca[Al_3(OH)_6(PO_3OH)(PO_4)]$, structure[8] and substituted Fe for Al, Ca for Ca, and P for P for one crandallite sheet. A trial β synthesis[9] using only those reflections which satisfied the subcell resulted in a map with highly prolate elliptical contours, the major axes of which were parallel to a^*.

Centric tests were not conclusive; we assumed the elliptical contours resulted from an acentric arrangement and repeated the β synthesis in space group Aa. Displacements in the contours away from x = $^1/_4$ resulted in more uniform spherical shapes and a new set of parameters led to R = 0.33 for the substructure. It was then apparent that trial bond distances between the Fe atoms indicated an edge-sharing octahedral sheet structure, not a corner-sharing sheet as found in crandallite. Guided by bond distances, intuition, and the chemical analysis, we assigned nine nonequivalent Fe atoms at $x \sim {}^1/_4$, three P at $x \sim {}^1/_4$, three P at $x \sim 0.11$, three P at $x \sim 0.39$, three Ca at $x \sim 0.08$, and three Ca at $x \sim 0.42$ and repeated the β synthesis with all reflections for the full mitridatite cell. Although R = 0.50 at this stage, it was possible to locate all oxygens associated with the FeO_6 octahedra and PO_4 tetrahedra. A trial β synthesis led to R = 0.33 after slight readjustment of the atomic coordinate parameters. At this stage, blocked least-squares refinement of these coordinates (B set to 1.0 Å^{-2}) led to convergence at R = 0.22. A difference Fourier synthesis revealed six oxygens coordinated to Ca only and three oxygens in open spaces and we assumed these to be water molecules. Further convergence was rapid.

Four cycles of scale factor, s ($F_o = sF_c$), coefficient of secondary extinction,[10] atomic coordinate parameter, isotropic thermal vibration parameter refinements led to excellent convergence at R = 0.068 and R_w = 0.082, where,

$$R = \frac{\Sigma \| F_o | - | F_c \|}{\Sigma | F_o |}$$

$$R_w = \left[\frac{\Sigma_w (| F_o | - | F_c |)^2}{\Sigma_w F_o^2} \right]^{1/2}$$

The final cycle minimized $\sum w||F_o| - |F_c||^2$ where $w = \sigma^{-2}(F)$. The "goodness of fit", $S = \sum w||F_o| - |F_c||^2/(n-m)$, where n = number of independent F's and m = number of parameters, was set at 1.00 in final refinement and w adjusted such that $\sigma^{-2}(F) = \sigma^2 F(\text{old}) + kF_o^2$. The total number of parameters was m = 302, so the independent data to variable parameter ratio is about 18:1.

We employed scattering curves[11] for Ca^{2+}, Fe^{3+}, P^{5+}, and O^{1-} and applied anomalous dispersion corrections[12] to Fe, P, and Ca.

A final difference synthesis revealed a low profile with no evidence of remaining non-hydrogen atoms and it was not possible to directly ascertain the hydrogen atom locations, doubtless owing to the rather dense matrix and pronounced pseudosymmetry of mitridatite. Atomic coordinate parameters and isotropic thermal vibration parameters are presented in Table II. It is seen that the thermal parameters range between 0.58 and 0.69 Å for Fe, 0.78 and 1.09 Å^{-2} for Ca, 0.53 and 0.61 Å^{-2} for P, and 0.34 and 2.4 Å^{-2} for O, typical values for a dense and well-ordered crystal structure. Pertinent bond distances and angles are given in Table III.

The condensed discussion above can hardly convey the unusual complexity of the structure study which spanned 3 years and which required at least 50 β syntheses. Indeed 9 Fe, 6 P, 6 Ca, and 24 O^{2-} approximate in position those found in a sheet of crandallite and dictate the substructure. The essential difficulty, however, was in assigning correct phase angles for the majority of structure factors which were relatively weak and which were mainly influenced by the additional 3 P, 18 O^{2-}, and 9 OW (=H_2O) atoms in the asymmetric unit. These latter amount to 28% of the total scattering matter, too great for correct phasing by the substructure reflections and too small for location on the $P(uvw)$ map. The correct formula for an asymmetric unit of mitridatite is $Ca_6(H_2O)_6[Fe^{III}_9O_6(PO_4)_9]\cdot 3H_2O$.

Description of the Structure

The Octahedral Sheet. The underlying structural principle for mitridatite is an elegant compact sheet of composition $[Fe^{III}_9O_6(PO_4)_9]^{12-}$ (Figure 1) oriented parallel to the {100} plane and situated at $x \sim {}^1/_4$ and $^3/_4$. The complex cell of low symmetry masquerades a pronounced trigonal pseudosymmetry with two-sided plane group $p31m$, a = 11.25 Å (=c of the mitridatite cell). The sheet is built up of octahedral edge-sharing nonamers each defining a trigonal ring which fuse

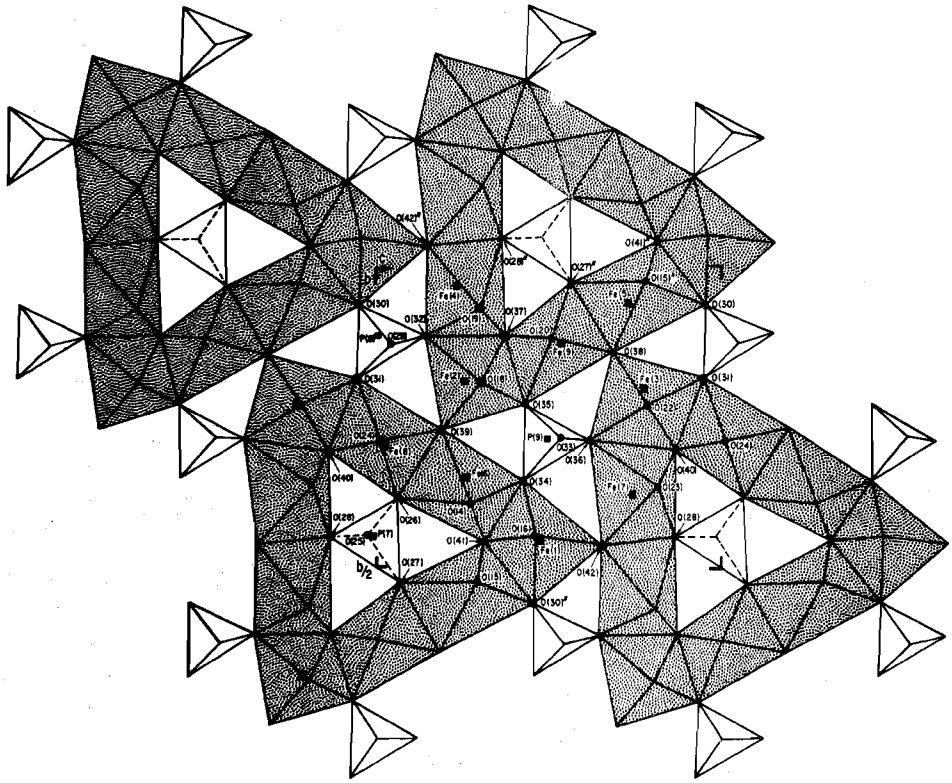

Figure 1. The $[Fe_9O_6(PO_4)_9]^{12-}$ sheet in mitridatite. Atoms are labeled to conform with Table II.

at their extreme trigonal corners to the edge midpoints of symmetry equivalent nonamers. These nonamers have composition $M_9\phi_{36}$ (where M = octahedral center and ϕ = vertex) and constitute an asymmetric unit of structure, the condensed octahedral sheet having composition $M_9\phi_{33}$. The point of condensation is an oxo anion (O^{2-}) which is bonded to three Fe^{3+} ions. In addition, each nonamer possesses three corners in its interior, also comprised of oxo anions, which are also bonded to three Fe^{3+} ions. At the center of each nonamer is a (PO_4) tetrahedron along a pseudotrigonal axis which is linked at three of its corners to octahedra and we refer to its center as P(a). It is located at the origin of the $p31m$ pseudocell. The assembled sheet has a second kind of pseudotrigonal axis which also passes through (PO_4) tetrahedra, the centers of which we designate P(b). They are located at $^1/_3{}^2/_3z$ and $^2/_3{}^1/_3z$ positions of the $p31m$ pseudocell. Finally, (PO_4) tetrahedra link at three of their corners to triangular groupings of octahedral vertices above and below the sheet and these we call P(c). Thus, the sheet formula can be written, $[Fe^{III}{}_9O_6(P(a)O_4)(P(b)O_4)_2(P(c)O_4)_6]^{12-}$.

The nonamer can be directly related to the central girdle of the well-known Keggin molecule, of which $[PW_{12}O_{40}]^{3-}$ is an example, by removing the trigonal edge-sharing caps above and below the molecule resulting in $[PW_6O_{28}]$. It is topologically identical to the central girdle of the related $[PMo_9O_{31}(H_2O)_3]^{3-}$ polyanion which has been shown[13] to be related to the Keggin molecule. Rewriting this polyanion $[(PMo_6O_{28})Mo_3O_3(H_2O)_3]$, mitridatite's isomorphic region can be written $[P(a)Fe_6O_{28}]$; it is obtained by removing the three octahedra at the extreme trigonal corners of the nonamer (Figure 2).

The sheet in mitridatite appeared quite new to us until a local isomorphism was discovered between it and the seemingly unrelated schairerite structure,[14] $Na_{21}F_6Cl(SO_4)_7$, $P31m$, Z = 3, a = 12.20 Å, c = 19.26 Å. This latter compound is based on the compression of seven trigonal sheets within the c-axial repeat, one of which is geometrically isomorphic to mitridatite. In schairerite, the isomorphic sheet has composition

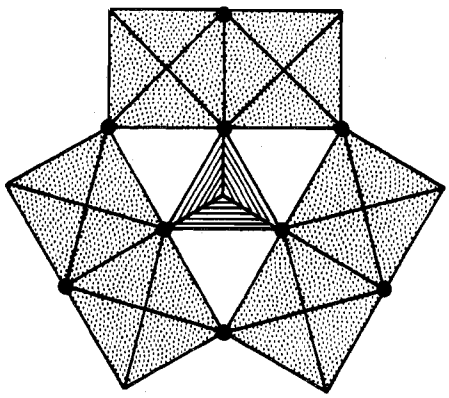

Figure 2. The $[PFe_6O_{28}]$ central girdle found in the Keggin molecule and in mitridatite.

$[Na_9F_6(SO_4)_9]^{15-}$ and conserves every geometrical detail of the mitridatite sheet including the orientations of the tetrahedra. The remaining six sheets in schairerite share local isomorphisms with the curious crystal structure of långbanite, $Mn^{II}{}_4Mn^{III}{}_9Sb^{V}Si^{IV}{}_2O_{24}$, $P31m$, Z = 3, a = 11.57 Å, c = 11.12 Å. Our presently unpublished results show that långbanite possesses four sheets in the c-axial repeat, two of which are isomorphic to sheets in schairerite, viz., $Mn^{II}{}_{12}Mn^{III}{}_9Sb^{V}{}_3[Mn^{III}{}_9O_{24}(SiO_4)_3]_2$. The composition in brackets constitutes the isomorphic region and the remaining cations are organized in an ordered way according to the sheet of the familiar brucite, $Mg(OH)_2$, structure type.

Perhaps most intriguing is the fact that mitridatite is a collapsed version of the crystal structure of the well-known alunite structure type and the crandallite isotype.[8,15] The comparison is best made by following the trigonal idealizations of the structures in Figure 3. The alunite structure type is built of a corner-linked octahedral sheet which is based on three-membered and six-membered octahedral rings (Figure 3a). The octahedral centers define the vertices of the well-known Kagomé net. If alternate three-membered octahedral

Table II. Mitridatite Atomic Coordinate Parameters[a]

	x	y	z	B, Å²
Fe(1)	0.2500	0.46266 (8)	0.5000	0.60 (2)
Fe(2)	0.2465 (1)	0.20013 (8)	0.2917 (2)	0.58 (2)
Fe(3)	0.2468 (1)	0.22755 (8)	0.7935 (2)	0.60 (2)
Fe(4)	0.2434 (1)	0.04173 (8)	0.2716 (2)	0.60 (2)
Fe(5)	0.2456 (1)	0.05241 (8)	0.7703 (2)	0.62 (2)
Fe(6)	0.2487 (1)	0.37474 (8)	0.2725 (2)	0.69 (2)
Fe(7)	0.2517 (1)	0.38608 (8)	0.7719 (2)	0.65 (2)
Fe(8)	0.2504 (1)	0.29595 (8)	0.0397 (2)	0.64 (2)
Fe(9)	0.2401 (1)	0.12921 (8)	0.5377 (2)	0.60 (2)
Ca(1)	0.5807 (2)	0.0376 (1)	0.8212 (2)	0.97 (6)
Ca(2)	0.5820 (2)	0.1717 (1)	0.3670 (2)	0.78 (5)
Ca(3)	0.5762 (2)	0.3737 (1)	0.8394 (2)	0.91 (5)
Ca(4)	0.4155 (2)	0.2880 (1)	0.2319 (2)	0.88 (6)
Ca(5)	0.4157 (2)	0.4858 (1)	0.6851 (2)	1.09 (6)
Ca(6)	0.4125 (2)	0.1551 (1)	0.7090 (2)	0.95 (5)
P(1)	0.1052 (2)	0.2863 (1)	0.1836 (3)	0.53 (4)
O(1)	0.0198 (5)	0.2852 (4)	0.1686 (7)	1.17 (12)
O(2)	0.1369 (5)	0.2206 (4)	0.2533 (7)	0.97 (13)
O(3)	0.1382 (5)	0.3498 (4)	0.2549 (7)	0.95 (12)
O(4)	0.1401 (5)	0.2863 (4)	0.0616 (6)	0.58 (11)
P(2)	0.1054 (2)	0.4618 (1)	0.6459 (3)	0.61 (4)
O(5)	0.0191 (5)	0.4578 (4)	0.6282 (7)	1.06 (12)
O(6)	0.1351 (5)	0.5279 (4)	0.7148 (7)	0.81 (12)
O(7)	0.1390 (5)	0.3988 (4)	0.7194 (7)	0.81 (11)
O(8)	0.1398 (5)	0.4613 (4)	0.5235 (7)	1.02 (12)
P(3)	0.1018 (2)	0.1440 (1)	0.6894 (2)	0.56 (4)
O(9)	0.0162 (5)	0.1466 (5)	0.6800 (7)	1.17 (13)
O(10)	0.1371 (5)	0.2082 (4)	0.7602 (7)	1.02 (12)
O(11)	0.1326 (5)	0.0775 (4)	0.7547 (7)	0.98 (12)
O(12)	0.1312 (5)	0.1444 (4)	0.5626 (7)	1.14 (13)
P(4)	0.3932 (2)	0.4660 (1)	0.3548 (3)	0.57 (4)
O(13)	0.4792 (5)	0.4691 (4)	0.3607 (7)	0.74 (11)
O(14)	0.3629 (5)	0.3976 (4)	0.2918 (7)	0.75 (11)
O(15)	0.3584 (5)	0.5290 (4)	0.2855 (7)	0.75 (11)
O(16)	0.3654 (5)	0.4667 (4)	0.4820 (7)	0.72 (11)
P(5)	0.3889 (2)	0.1192 (1)	0.3965 (3)	0.58 (4)
O(17)	0.4739 (5)	0.1166 (4)	0.4165 (7)	0.95 (12)
O(18)	0.3602 (5)	0.1863 (4)	0.3271 (6)	0.66 (11)
O(19)	0.3568 (5)	0.0559 (4)	0.3205 (7)	0.88 (12)
O(20)	0.3542 (5)	0.1186 (4)	0.5190 (7)	0.87 (12)
P(6)	0.3943 (2)	0.3085 (1)	0.8955 (3)	0.57 (4)
O(21)	0.4811 (5)	0.3098 (4)	0.9072 (7)	0.82 (11)
O(22)	0.3628 (5)	0.2430 (4)	0.8255 (7)	0.83 (11)
O(23)	0.3626 (5)	0.3736 (4)	0.8265 (7)	0.95 (12)
O(24)	0.3638 (5)	0.3075 (4)	1.0209 (7)	0.77 (11)
P(7)	0.2067 (2)	0.4590 (1)	1.0165 (3)	0.56 (4)
O(25)	0.1230 (6)	0.4449 (5)	0.9905 (8)	1.45 (14)
O(26)	0.2489 (5)	0.3993 (4)	1.0927 (6)	0.34 (10)
O(27)	0.2286 (5)	0.5276 (4)	1.0880 (7)	0.99 (13)
O(28)	0.2453 (5)	0.4637 (4)	0.8979 (7)	0.60 (11)
P(8)	0.2871 (2)	0.1280 (1)	1.0370 (3)	0.57 (4)
O(29)	0.3720 (6)	0.1190 (5)	1.0593 (8)	1.41 (14)
O(30)	0.2501 (5)	0.0688 (5)	0.9587 (7)	1.15 (13)
O(31)	0.2579 (5)	0.1954 (4)	0.9751 (7)	0.77 (11)
O(32)	0.2472 (5)	0.1265 (4)	1.1557 (7)	0.82 (11)
P(9)	0.2876 (2)	0.2942 (1)	0.5364 (3)	0.60 (4)
O(33)	0.3724 (6)	0.2845 (5)	0.5560 (8)	1.45 (14)
O(34)	0.2595 (4)	0.3581 (4)	0.4598 (6)	0.62 (11)
O(35)	0.2478 (5)	0.2303 (4)	0.4726 (7)	0.94 (12)
O(36)	0.2515 (5)	0.3014 (4)	0.6550 (7)	0.98 (12)
O(37)	0.2137 (4)	0.1142 (4)	0.3709 (6)	0.59 (11)
O(38)	0.2726 (5)	0.1452 (4)	0.7107 (7)	0.82 (11)
O(39)	0.2771 (5)	0.2827 (4)	0.2143 (6)	0.68 (11)
O(40)	0.2205 (4)	0.3138 (4)	0.8757 (6)	0.47 (10)
O(41)	0.2191 (4)	0.4639 (4)	0.3250 (6)	0.51 (10)
O(42)	0.2773 (5)	0.4650 (4)	0.6680 (7)	0.81 (11)
OW(1)	0.4990 (6)	0.2693 (5)	0.4121 (8)	1.35 (13)
OW(2)	0.4856 (6)	0.3789 (5)	0.6597 (8)	1.84 (15)
OW(3)	0.4981 (5)	0.0616 (5)	0.6506 (7)	1.14 (13)
OW(4)	0.4926 (6)	0.1928 (5)	0.1842 (8)	1.49 (14)
OW(5)	0.5022 (6)	0.4707 (4)	0.8748 (8)	1.17 (13)
OW(6)	0.4891 (6)	0.1222 (5)	0.8916 (8)	1.81 (16)
OW(7)	0.4275 (6)	0.4509 (5)	0.0628 (9)	1.64 (15)
OW(8)	0.5775 (6)	0.3798 (6)	0.4874 (9)	2.18 (17)
OW(9)	0.5812 (7)	0.2132 (6)	0.0080 (9)	2.39 (18)

[a] Estimated standard errors in parentheses refer to the last digit.

rings are collapsed together to form an edge-sharing system, the mitridatite configuration obtains (Figure 3b). The six-membered rings now become triangular regions which receive the $P(a)O_4$ and $P(b)O_4$ tetrahedra. A further collapse (Figure 3c) leads to the edge-sharing Kagomé sheet of octahedra, well-known as a slice of spinel along the {111} plane and found as an entity in the crystal structure of chloritoid,[16] $Fe_2Al(OH)_4[Al_3O_2(SiO_4)_2]$. This is the densest sheet possible since it is a section of the cubic close-packing (·c·). Thus, a progressive sequence of sheets of increasing density can be conceived, beginning with the iron phosphate isotype of alunite, lusungite:

	Sheet	% collapse (area)
Lusungite	$[Fe_9(OH)_{18}(P(c)O_4)_6]^{9-}$	0.0
Mitridatite	$[Fe_9O_6(P(a)O_4)(P(b)O_4)_2(P(c)O_4)_6]^{12-}$	16.1
Hypothetical	$[Fe_9O_6(P(a)O_4)_3(P(b)O_4)_3]^{3-}$	35.1

To assess the degree of collapse based on the area of the cells, the cell length of the hypothetical condensed structure, $3\text{-}[M_3O_2(TO_4)_2]$, was derived by isomorphic substitution of Fe^{3+} for Al^{3+} in chloritoid. It is noted that mitridatite affords a reduction of about 16% in area and the hypothetical sheet composition an additional 19%. Among phosphates, the hypothetical sheet has yet to be found although it appears in bermanite, $Mn^{II}(H_2O)_4[\square Mn^{III}_2(OH)_2(PO_4)_2]$, if the ordered vacancy, □, is included.[17]

In all three structures, the loci of the Fe atoms are approximately the same which accounts for similar substructure reflections. Thus, the progressive condensation of the sheets outlined above is an interesting example of oxygen rearrangements about the same configuration of metal centers. The $P(c)O_4$ tetrahedra in the lusungite and mitridatite structures are also approximately isomorphic as seen in Figure 4, the tetrahedra for the former represented by the isomorphic crandallite parameters.[8] Although mitridatite was earlier suggested to be related in some way to the alunite structure,[18] the contradiction of a decrease in area where an increase was expected through isomorphic substitution of Al^{3+} by Fe^{3+} can now be understood; mitridatite is a new type chemically and structurally, topologically distinct from but related to alunite.

The Alkaline Earth–Water Layer. A thick assembly of $CaO_5(H_2O)_2$ polyhedra and water molecules occurs as open sheets parallel to {100} at about $x \sim 0$ and $^1/_2$. A polyhedral diagram about $x \sim {}^1/_2$ is featured in Figure 5. All six nonequivalent $CaO_5(H_2O)_2$ polyhedra possess approximately the same geometry; each Ca is coordinated to four phosphate oxygens, one oxo anion, and two water molecules, defining a distorted octahedron with an additional coordination sphere above the midpoint of one of the octahedral faces. In Figure 6, the polyhedron is featured with its vertices classified ac-

Table III. Mitridatite Polyhedral Interatomic Distances (Å) and Angles (deg)[a,e]

Fe(1)			Fe(2)			Fe(3)		
a Fe(1)-O(41)	1.989 (7)		Fe(2)-O(37)	1.999 (7)		Fe(3)-O(40)	1.985 (7)	
b Fe(1)-O(42)	1.902 (8)		Fe(2)-O(39)	1.923 (8)		Fe(3)-O(38)	1.923 (8)	
e Fe(1)-O(16)	2.057 (8)		Fe(2)-O(18)	2.012 (8)		Fe(3)-O(22)	2.053 (8)	
e Fe(1)-O(8)	1.979 (9)		Fe(2)-O(2)	1.969 (9)		Fe(3)-O(10)	1.961 (9)	
d Fe(1)-O(34)	2.083 (8)		Fe(2)-O(32)	2.092 (8)		Fe(3)-O(31)	2.125 (7)	
d Fe(1)-O(30)″	2.106 (9)		Fe(2)-O(35)	2.115 (8)		Fe(3)-O(36)	2.122 (8)	
Average	2.019		Average	2.018		Average	2.028	
O(30)″-O(41)	2.554 (11)[b]	77.1 (3)	O(32)-O(37)	2.560 (10)[b]	77.4 (3)	O(31)-O(40)	2.604 (11)[b]	78.6 (3)
O(34)-O(41)	2.602 (10)[b]	79.4 (3)	O(35)-O(37)	2.565 (11)[b]	77.1 (3)	O(36)-O(40)	2.605 (10)[b]	78.7 (3)
O(16)-O(42)	2.724 (11)[c]	86.9 (3)	O(18)-O(39)	2.616 (11)[c]	83.3 (3)	O(22)-O(38)	2.708 (11)[c]	85.8 (3)
O(8)-O(41)	2.749 (11)[c]	87.7 (3)	O(2)-O(37)	2.729 (11)[c]	86.9 (3)	O(10)-O(40)	2.762 (11)[c]	88.8 (3)
O(8)-O(42)	2.771 (12)	91.1 (4)	O(2)-O(39)	2.812 (12)	92.6 (3)	O(22)-O(31)	2.773 (11)	83.2 (3)
O(16)-O(34)	2.800 (11)	85.1 (3)	O(18)-O(35)	2.820 (11)	86.2 (3)	O(10)-O(38)	2.780 (12)	91.4 (4)
O(16)-O(30)″	2.821 (12)	85.3 (3)	O(18)-O(32)	2.866 (11)	88.5 (3)	O(22)-O(36)	2.831 (11)	85.4 (3)
O(16)-O(41)	2.966 (11)	94.3 (3)	O(2)-O(32)	2.951 (12)	93.2 (3)	O(22)-O(40)	2.953 (11)	94.0 (3)
O(8)-O(30)″	2.983 (12)	93.7 (3)	O(2)-O(35)	2.988 (12)	94.0 (3)	O(10)-O(36)	3.029 (12)	95.7 (3)
O(8)-O(34)	3.036 (12)	96.7 (3)	O(18)-O(37)	3.009 (11)	97.2 (3)	O(10)-O(31)	3.060 (11)	96.9 (3)
O(30)″-O(42)	3.095 (11)	100.9 (3)	O(32)-O(39)	3.128 (11)	102.3 (3)	O(36)-O(38)	3.102 (11)	100.0 (3)
O(34)-O(42)	3.116 (10)	102.8 (3)	O(35)-O(39)	3.169 (10)	103.3 (3)	O(31)-O(38)	3.164 (10)	102.7 (3)
Average	2.851	90.1	Average	2.851	90.2	Average	2.864	90.1

Fe(4)			Fe(5)			Fe(6)		
a Fe(4)-O(37)	1.898 (7)		Fe(5)-O(41)″	1.895 (7)		Fe(6)-O(41)	1.912 (7)	
b Fe(4)-O(42)″	2.015 (8)		Fe(5)-O(38)	1.991 (8)		Fe(6)-O(39)	1.979 (8)	
e Fe(4)-O(19)	2.030 (9)		Fe(5)-O(15)″	2.021 (8)		Fe(6)-O(14)	2.043 (8)	
e Fe(4)-O(6)″	1.961 (9)		Fe(5)-O(11)	2.033 (9)		Fe(6)-O(3)	1.989 (9)	
c Fe(4)-O(28)″	2.071 (7)		Fe(5)-O(27)″	2.097 (8)		Fe(6)-O(26)	2.077 (7)	
d Fe(4)-O(32)	2.101 (8)		Fe(5)-O(30)	2.137 (8)		Fe(6)-O(34)	2.120 (7)	
Average	2.013		Average	2.029		Average	2.020	
O(32)-O(37)	2.560 (10)[b]	79.4 (3)	O(30)-O(41)″	2.554 (11)[b]	78.3 (3)	O(34)-O(41)	2.602 (10)[b]	80.2 (3)
O(6)″-O(37)	2.699 (11)[c]	88.8 (3)	O(27)″-O(38)	2.732 (11)[b]	83.8 (3)	O(26)-O(39)	2.658 (10)[b]	81.8 (3)
O(28)″-O(42)″	2.702 (10)[b]	82.8 (3)	O(11)-O(41)″	2.743 (11)[c]	88.5 (3)	O(3)-O(41)	2.698 (11)[c]	87.5 (3)
O(19)-O(42)″	2.738 (11)[c]	85.2 (3)	O(15)″-O(38)	2.789 (11)[c]	88.1 (3)	O(14)-O(39)	2.776 (11)[c]	87.3 (3)
O(19)-O(28)″	2.850 (11)	88.0 (3)	O(11)-O(27)″	2.816 (12)	86.0 (3)	O(3)-O(39)	2.840 (11)	91.4 (3)
O(19)-O(37)	2.863 (12)	93.5 (3)	O(15)″-O(41)″	2.827 (11)	92.4 (3)	O(14)-O(26)	2.847 (11)	87.4 (3)
O(6)″-O(32)	2.867 (12)	89.7 (3)	O(11)-O(38)	2.873 (12)	91.1 (3)	O(14)-O(34)	2.854 (10)	86.5 (3)
O(6)″-O(42)″	2.874 (12)	92.6 (3)	O(11)-O(30)	2.930 (12)	89.2 (3)	O(14)-O(41)	2.890 (11)	93.8 (3)
O(19)-O(32)	2.878 (11)	88.3 (3)	O(27)″-O(41)″	2.957 (10)	95.4 (3)	O(3)-O(26)	2.957 (11)	93.3 (3)
O(6)″-O(28)″	2.953 (11)	94.1 (3)	O(15)″-O(30)	2.960 (11)	90.7 (3)	O(3)-O(34)	2.979 (11)	92.9 (3)
O(28)″-O(37)	2.975 (11)	97.0 (3)	O(15)″-O(27)″	3.017 (12)	94.2 (3)	O(26)-O(41)	2.990 (10)	97.0 (3)
O(32)-O(42)″	3.170 (11)	100.7 (3)	O(30)-O(38)	3.218 (11)	102.4 (3)	O(34)-O(39)	3.166 (10)	101.1 (3)
Average	2.844	90.0	Average	2.868	90.0	Average	2.855	90.0

Fe(7)			Fe(8)			Fe(9)		
a Fe(7)-O(40)	1.936 (7)		Fe(8)-O(40)	1.897 (7)		Fe(9)-O(37)	1.908 (7)	
b Fe(7)-O(42)	2.002 (8)		Fe(8)-O(39)	1.989 (7)		Fe(9)-O(38)	1.996 (7)	
e Fe(7)-O(23)	1.994 (9)		Fe(8)-O(24)	2.037 (8)		Fe(9)-O(20)	2.044 (9)	
e Fe(7)-O(7)	2.023 (8)		Fe(8)-O(4)	1.985 (8)		Fe(9)-O(12)	1.982 (9)	
c Fe(7)-O(28)	2.076 (8)		Fe(8)-O(26)	2.088 (7)		Fe(9)-O(27)″	2.062 (8)	
d Fe(7)-O(36)	2.100 (8)		Fe(8)-O(31)	2.085 (8)		Fe(9)-O(35)	2.098 (8)	
Average	2.022		Average	2.014		Average	2.015	
O(36)-O(40)	2.605 (10)[b]	80.3 (3)	O(31)-O(40)	2.604 (11)[b]	81.5 (3)	O(35)-O(37)	2.565 (11)[b]	79.5 (3)
O(28)-O(42)	2.702 (10)[b]	83.0 (3)	O(26)-O(39)	2.658 (10)[b]	81.4 (3)	O(27)″-O(38)	2.732 (11)[b]	84.6 (3)
O(7)-O(40)	2.709 (11)[c]	86.3 (3)	O(4)-O(40)	2.692 (10)[c]	87.8 (3)	O(20)-O(38)	2.755 (11)[c]	86.0 (3)
O(23)-O(42)	2.828 (11)[c]	90.1 (3)	O(4)-O(39)	2.810 (11)	90.0 (3)	O(12)-O(37)	2.779 (11)[c]	91.2 (3)
O(7)-O(42)	2.856 (12)	90.4 (3)	O(24)-O(39)	2.821 (10)[c]	89.0 (3)	O(12)-O(27)″	2.830 (12)	88.8 (4)
O(23)-O(40)	2.856 (11)	93.1 (3)	O(24)-O(40)	2.859 (11)	93.2 (3)	O(20)-O(37)	2.832 (11)	91.5 (3)
O(23)-O(28)	2.873 (12)	89.8 (3)	O(24)-O(26)	2.865 (11)	88.0 (3)	O(12)-O(38)	2.845 (12)	91.3 (3)
O(7)-O(36)	2.876 (12)	88.4 (3)	O(24)-O(31)	2.869 (11)	88.2 (3)	O(20)-O(35)	2.869 (12)	87.7 (3)
O(7)-O(28)	2.886 (11)	89.5 (3)	O(4)-O(26)	2.902 (11)	90.8 (3)	O(12)-O(35)	2.898 (12)	90.5 (3)
O(28)-O(40)	2.940 (10)	94.2 (3)	O(26)-O(40)	2.949 (10)	95.3 (3)	O(27)″-O(37)	2.951 (10)	96.0 (3)
O(23)-O(36)	2.951 (11)	92.2 (3)	O(4)-O(31)	2.954 (11)	93.0 (3)	O(20)-O(27)″	2.986 (12)	93.3 (3)
O(36)-O(42)	3.199 (11)	102.5 (3)	O(31)-O(39)	3.165 (10)	101.9 (3)	O(35)-O(38)	3.136 (10)	100.0 (3)
Average	2.857	90.0	Average	2.846	90.0	Average	2.848	90.0

Ca(1)		Ca(2)		Ca(3)	
g		Ca(2)-O(17)	2.293 (9)		
g′ Ca(1)-O(13)″	2.300 (8)			Ca(3)-O(21)	2.272 (8)
a Ca(1)-O(41)′	2.425 (8)	Ca(2)-O(40)′	2.440 (8)	Ca(3)-O(37)′	2.415 (8)
e Ca(1)-O(3)′	2.544 (9)	Ca(2)-O(10)′	2.832 (9)	Ca(3)-O(6)‴	2.637 (8)
e Ca(1)-O(8)′	2.403 (9)	Ca(2)-O(4)′	2.457 (8)	Ca(3)-O(12)′	2.620 (8)
e Ca(1)-O(11)‴	2.548 (9)	Ca(2)-O(7)′	2.440 (8)	Ca(3)-O(12)′	2.369 (9)
h Ca(1)-OW(6)	2.480 (10)	Ca(2)-OW(1)	2.469 (10)	Ca(3)-OW(5)	2.341 (9)
h Ca(1)-OW(3)	2.331 (9)	Ca(2)-OW(4)	2.490 (10)	Ca(3)-OW(2)	2.443 (10)
Average	2.433	Average	2.489	Average	2.442

Ca(1) (*Continued*)	
O(3)′–O(41)′	2.698 (11)[c]
O(11)′–O(41)′	2.743 (11)[c]
O(8)′–O(41)′	2.749 (11)[d]
OW(3)–OW(6)	2.973 (11)[d]
O(13)″–OW(6)	2.986 (12)
O(13)″–OW(3)	3.011 (11)
O(3)′–OW(3)	3.126 (12)
O(11)‴–O(13)″	3.184 (12)
O(3)′–OW(6)	3.213 (13)
O(8)′–OW(6)	3.317 (13)
O(8)′–O(13)″	3.473 (12)
O(11)‴–OW(3)	3.692 (13)
O(3)′–O(8)′	3.711 (13)
O(8)′–O(11)‴	3.760 (13)
O(3)′–O(11)‴	4.408 (14)
Average	3.270

Ca(2) (*Continued*)	
O(4)′–O(40)′	2.692 (10)[c]
O(7)′–O(40)′	2.709 (11)[c]
O(10)′–O(40)′	2.762 (11)[c]
OW(1)–OW(4)	2.951 (12)[d]
O(17)–OW(1)	2.988 (12)
O(4)′–OW(1)	3.044 (12)
O(17)–OW(4)	3.047 (11)
O(7)′–OW(4)	3.114 (13)
O(10)′–OW(1)	3.134 (13)
O(10)′–OW(4)	3.224 (13)
O(4)′–O(17)	3.706 (13)
O(4)′–O(10)′	3.707 (13)
O(7)′–O(10)′	3.718 (13)
O(7)′–O(17)	3.835 (13)
O(4)′–O(7)′	4.421 (14)
Average	3.270

Ca(3) (*Continued*)	
O(6)‴–O(37)′	2.699 (11)[c]
O(2)′–O(37)′	2.729 (11)[c]
O(12)′–O(37)′	2.779 (11)[c]
OW(2)–OW(5)	2.992 (11)[d]
O(6)‴–OW(5)	3.088 (12)
O(21)–OW(2)	3.096 (12)
O(21)–O(12)′	3.140 (12)
O(21)–OW(5)	3.162 (12)
O(6)‴–OW(2)	3.192 (13)
O(2)′–OW(2)	3.361 (13)
O(2)′–O(21)	3.433 (12)
O(12)′–OW(5)	3.685 (13)
O(2)′–O(6)‴	3.754 (13)
O(2)′–O(12)′	3.789 (13)
O(6)‴–O(12)′	4.522 (14)
Average	3.295

Ca(4)		
g		
g′ Ca(4)–O(9)′	2.297 (9)	
a Ca(4)–O(39)	2.420 (8)	
e Ca(4)–O(18)	2.485 (8)	
e Ca(4)–O(14)	2.434 (8)	
e Ca(4)–O(24)	2.482 (8)	
h Ca(4)–OW(1)	2.405 (9)	
h Ca(4)–OW(4)	2.380 (10)	
Average	2.415	
O(18)–O(39)	2.616 (11)[c]	
O(14)–O(39)	2.776 (11)[c]	
O(24)–O(39)	2.821 (10)[c]	
OW(1)–OW(4)	2.951 (12)[d]	
O(18)–OW(4)	2.960 (12)	
O(18)–OW(1)	2.993 (12)	
O(9)′–OW(1)	3.117 (12)	
O(9)′–OW(4)	3.137 (13)	
O(9)′–O(24)	3.190 (12)	
O(9)′–O(14)	3.199 (12)	
O(14)–O(24)	3.512 (11)	
O(24)–OW(4)	3.546 (13)	
O(14)–OW(1)	3.612 (13)	
O(14)–O(18)	4.109 (14)	
O(18)–O(24)	4.173 (14)	
Average	3.247	

Ca(5)		
Ca(5)–O(5)‴	2.265 (9)	
Ca(5)–O(42)	2.451 (9)	
Ca(5)–O(23)	2.900 (8)	
Ca(5)–O(19)″	2.356 (8)	
Ca(5)–O(16)	2.392 (8)	
Ca(5)–OW(5)	2.507 (9)	
Ca(5)–OW(2)	2.437 (10)	
Average	2.473	
O(16)–O(42)	2.724 (11)[c]	
O(19)″–O(42)	2.738 (11)[c]	
O(23)–O(42)	2.828 (11)[c]	
OW(2)–OW(5)	2.992 (11)[d]	
O(23)–OW(2)	3.003 (13)	
O(19)″–OW(5)	3.047 (13)	
O(23)–OW(5)	3.093 (13)	
O(5)‴–OW(5)	3.141 (12)	
O(16)–OW(2)	3.238 (12)	
O(5)‴–OW(2)	3.241 (13)	
O(5)‴–O(16)	3.348 (12)	
O(9)″–O(23)	3.529 (12)	
O(5)‴–O(19)″	3.757 (13)	
O(16)–O(19)″	4.197 (14)	
O(16)–O(23)	4.278 (14)	
Average	3.277	

Ca(6)		
Ca(6)–O(1)′	2.294 (9)	
Ca(6)–O(38)	2.465 (9)	
Ca(6)–O(15)″	2.786 (8)	
Ca(6)–O(22)	2.368 (8)	
Ca(6)–O(20)	2.381 (8)	
Ca(6)–OW(6)	2.424 (10)	
Ca(6)–OW(3)	2.483 (9)	
Average	2.457	
O(22)–O(38)	2.708 (11)[c]	
O(20)–O(38)	2.755 (11)[c]	
O(15)″–O(38)	2.789 (11)[c]	
OW(3)–OW(6)	2.973 (11)[d]	
O(1)′–OW(3)	2.994 (13)	
O(20)–OW(3)	3.006 (12)	
O(15)″–OW(6)	3.063 (13)	
O(15)″–OW(3)	3.078 (12)	
O(1)′–OW(6)	3.174 (12)	
O(22)–OW(6)	3.256 (13)	
O(15)″–O(20)	3.457 (11)	
O(1)′–O(22)	3.464 (11)	
O(1)′–O(20)	3.708 (13)	
O(15)″–O(22)	4.166 (14)	
O(20)–O(22)	4.195 (14)	
Average	3.252	

P(1)		
g P(1)–O(1)	1.492 (9)	
g′		
e P(1)–O(2)	1.567 (9)	
e P(1)–O(3)	1.547 (9)	
e P(1)–O(4)	1.559 (7)	
Average	1.541	
O(2)–O(3)	2.501 (12)	106.8 (5)
O(3)–O(4)	2.502 (11)	107.3 (4)
O(2)–O(4)	2.509 (11)	106.8 (4)
O(1)–O(2)	2.510 (13)	110.3 (5)
O(1)–O(3)	2.533 (12)	112.9 (5)
O(1)–O(4)	2.535 (11)	112.4 (5)
Average	2.515	109.4

P(2)		
P(2)–O(5)	1.510 (9)	
P(2)–O(7)	1.554 (8)	
P(2)–O(6)	1.557 (8)	
P(2)–O(8)	1.559 (8)	
Average	1.545	
O(6)–O(7)	2.499 (12)	106.9 (5)
O(7)–O(8)	2.514 (11)	107.7 (5)
O(6)–O(8)	2.517 (11)	107.8 (5)
O(5)–O(7)	2.519 (12)	110.5 (5)
O(5)–O(8)	2.527 (12)	110.8 (5)
O(5)–O(6)	2.556 (12)	112.9 (5)
Average	2.522	109.4

P(3)		
P(3)–O(9)	1.496 (10)	
P(3)–O(11)	1.551 (9)	
P(3)–O(10)	1.568 (9)	
P(3)–O(12)	1.566 (8)	
Average	1.545	
O(9)–O(11)	2.513 (13)	111.1 (5)
O(11)–O(12)	2.516 (11)	107.7 (5)
O(9)–O(10)	2.519 (13)	110.6 (5)
O(9)–O(12)	2.523 (13)	111.0 (5)
O(10)–O(11)	2.530 (12)	108.4 (5)
O(10)–O(12)	2.535 (11)	108.0 (5)
Average	2.523	109.5

P(4)		
g		
g′ P(4)–O(13)	1.505 (9)	
e P(4)–O(14)	1.570 (8)	
e P(4)–O(15)	1.539 (8)	
e P(4)–O(16)	1.559 (8)	
Average	1.543	
O(13)–O(15)	2.489 (11)	109.7 (5)
O(15)–O(16)	2.510 (11)	108.2 (4)
O(14)–O(16)	2.521 (11)	107.3 (4)
O(13)–O(14)	2.523 (11)	110.2 (4)
O(13)–O(16)	2.532 (11)	111.4 (5)
O(14)–O(15)	2.546 (11)	109.9 (4)
Average	2.520	109.4

P(5)		
P(5)–O(17)	1.488 (9)	
P(5)–O(19)	1.565 (9)	
P(5)–O(18)	1.572 (8)	
P(5)–O(20)	1.563 (8)	
Average	1.547	
O(17)–O(20)	2.499 (12)	110.0 (5)
O(17)–O(19)	2.514 (12)	110.8 (5)
O(18)–O(19)	2.526 (12)	107.2 (4)
O(17)–O(18)	2.532 (12)	111.7 (5)
O(18)–O(20)	2.536 (11)	108.0 (4)
O(19)–O(20)	2.547 (11)	109.0 (5)
Average	2.526	109.4

P(6)		
P(6)–O(21)	1.515 (8)	
P(6)–O(22)	1.564 (8)	
P(6)–O(23)	1.553 (8)	
P(6)–O(24)	1.558 (8)	
Average	1.547	
O(21)–O(23)	2.509 (12)	109.7 (5)
O(22)–O(24)	2.526 (11)	108.0 (4)
O(22)–O(23)	2.529 (12)	108.4 (4)
O(21)–O(24)	2.531 (11)	110.9 (4)
O(23)–O(24)	2.531 (11)	108.9 (5)
O(21)–O(22)	2.538 (12)	111.0 (5)
Average	2.527	109.5

Table III (*Continued*)

P(7)			P(8)			P(9)		
f P(7)-O(25)	1.494 (11)		P(8)-O(29)	1.496 (10)		P(9)-O(33)	1.495 (10)	
c P(7)-O(26)	1.578 (8)		P(8)-O(30)	1.547 (9)		P(9)-O(35)	1.558 (9)	
c P(7)-O(28)	1.559 (8)		P(8)-O(31)	1.542 (8)		P(9)-O(34)	1.559 (8)	
c P(7)-O(27)	1.580 (9)		P(8)-O(32)	1.570 (8)		P(9)-O(36)	1.541 (8)	
Average	1.553		Average	1.539		Average	1.538	
O(25)-O(28)	2.506 (13)	110.3 (5)	O(31)-O(32)	2.454 (11)	104.1 (4)	O(35)-O(36)	2.466 (11)	105.4 (5)
O(26)-O(27)	2.509 (11)	105.2 (5)	O(30)-O(31)	2.460 (12)	105.6 (5)	O(34)-O(36)	2.472 (11)	105.8 (4)
O(27)-O(28)	2.514 (11)	106.4 (5)	O(30)-O(32)	2.485 (11)	105.8 (5)	O(34)-O(35)	2.488 (11)	105.9 (4)
O(26)-O(28)	2.516 (10)	106.7 (4)	O(29)-O(30)	2.512 (13)	111.3 (5)	O(33)-O(36)	2.517 (13)	112.0 (5)
O(25)-O(26)	2.544 (13)	111.8 (5)	O(29)-O(32)	2.545 (13)	112.2 (5)	O(33)-O(35)	2.519 (13)	111.2 (5)
O(25)-O(27)	2.605 (13)	115.9 (5)	O(29)-O(31)	2.590 (12)	117.0 (5)	O(33)-O(34)	2.587 (12)	115.8 (5)
Average	2.532	109.4	Average	2.508	109.3	Average	2.508	109.4

Hydrogen Bonds

h→f	
OW(1)→O(33)	2.895 (13)
OW(2)→O(33)	2.860 (13)
OW(3)→O(25)′	2.978 (13)
OW(4)→O(29)″	2.809 (13)
OW(5)″→O(25)′	2.880 (13)
OW(6)→O(29)″	2.929 (13)
Average	2.892
d(O-H···O) pred[6]	2.60
$\Delta p_0 = +0.66$[f]	

h→i	
OW(1)→OW(8)	2.638 (14)
OW(2)→OW(8)	2.644 (14)
OW(3)→OW(7)″	2.618 (13)
OW(4)→OW(9)″	2.671 (14)
OW(5)″→OW(7)″	2.627 (13)
OW(6)→OW(9)″	2.646 (15)
Average	2.641
d(O-H···O) pred[6]	2.76
$\Delta p_0 = +0.24$[f]	

OW(3)-OW(7)″-O(9)‴	99.2 (4)
OW(3)-OW(7)″-OW(5)″	85.9 (4)
OW(5)″-OW(7)″-O(9)‴	100.6 (4)
Average	95.2
OW(6)″-OW(9)″-OW(4)″	84.0 (4)
OW(6)″-OW(9)″-O(21)″	85.2 (4)
OW(4)″-OW(9)″-O(21)″	90.6 (4)
Average	86.6
OW(1)-OW(8)-OW(2)	83.8 (4)
OW(1)-OW(8)-O(13)	93.7 (4)
OW(2)-OW(8)-O(13)	89.3 (4)
Average	88.9

OW(5)″-O(25)′-OW(3)	75.1 (4)
OW(6)″-O(29)″-OW(4)″	76.6 (4)
OW(1)-O(33)-OW(2)	75.6 (4)
Average	75.8

i→g′	
OW(7)″→O(9)‴	2.703 (13)
OW(8)→O(13)	2.737 (13)
OW(9)″→O(21)′	2.732 (14)
Average	2.724
d(O-H···O) pred[6]	2.74
$\Delta p_0 = +0.30$[f]	

[a] Estimated standard deviations refer to the last digit. [b] Fe–Fe oxygen octahedral shared edges. [c] Fe–Ca oxygen polyhedral shared edges. [d] Ca–Ca oxygen polyhedral shared edges. [e] ′ = $^1/_2 + x, ^1/_2 - y, ^1/_2 + z$; ″ = $x, ^1/_2 + y, ^1/_2 + z$; ‴ = $^1/_2 + x, -y, z$ applied to coordinates in Table II. [f] Valence units.

cording to four kinds of oxygens (see under Bond Distances). The first, O_g, corresponds to apical P(c)O_4 oxygens. The P(c)–O_g distances are among the shortest for all six nonequivalent Ca atoms. The second type, O_e, corresponds to basal P(c)O_4 oxygens which are, in addition, bonded to the Fe atoms. These are arranged in a manner similar to that found in the alunite structure type. The third, O_a (or O_b), which is the additional coordinating sphere above the midpoint of the octahedral face, corresponds to an oxo anion in the octahedral sheets. Thus, Ca:P(c):O^{2-} (oxo-) = 1:1:1. Finally, there exist two water molecules, O_h. These water molecules define a shared OW–OW′ edge which is shared by two Ca atoms resulting in $Ca_2O_{10}(H_2O)_2$ dimers. The arrangement of these dimers in Figure 5 results in a destruction of trigonal symmetry, thus leading to the monoclinic cell in mitridatite. Note that the orthohexagonal unit is related by $3^{1/2}b \sim c$ which is the orthogonal expression of the trigonal pseudosymmetry. From these observations, it is tempting to suggest that a trigonal modification may exist in nature, differing from mitridatite in the manner in which the interlayer large cations are organized.

Hydrogen Bonds. A hydrogen bond network is proposed on geometrical grounds since it was not possible to resolve hydrogen atom positions on a difference synthesis. Figure 5 shows these bonds and the model proposed is entirely consistent with bond distances and tetrahedral geometry. Three sets of clustered configurations occur which are each geometrically equivalent. The apical oxygens, O(25), O(29), and O(33) to P(7), P(8), and P(9), respectively, each receive two bonds from water molecules bonded to the Ca atoms. In addition, OW(7) through OW(9), which participate in hydrogen bonding only, each receive two bonds from the aforementioned water molecules and donate one bond to a phosphate oxygen, the composite defining the base of a tetrahedral configuration. The remaining hydrogen is weakly bonded to a PO_4 tetrahedral base above (or below) the layer. Thus, OW(7), OW(8), and OW(9) duplicate in their arrangement the complementary pattern found for P(7), P(8), and P(9), respectively.

The atomic arrangement described above explains many physical properties noted for mitridatite. The perfect basal cleavage, parallel to {100}, is the plane of the water molecules and the octahedral sheets. Mitridatite is extremely pleochroic, deep greenish-brown for vibrations parallel to the sheets and pale greenish-yellow for vibrations normal to the sheets.[4] In addition, the indexes of refraction in the sheets ($n_{\beta,\gamma} \sim 1.85$) are considerably greater than the index normal to the sheets ($n_\alpha \sim 1.78$). These phenomena arise from the short Fe–Fe separations in the plane of the sheets owing to extensive edge sharing and it is predicted that the compound will possess extensive antiferromagnetic character with an anomalously low magnetic moment per Fe atom. Indeed, Rossman[19] found $\mu = 3.54\ \mu_B$ for jarosite at 298 K, and with the much shorter Fe–Fe separations found in mitridatite the magnetic moment is expected to be even further reduced in that mineral owing to spin coupling across shared edges.

Bond Distances and Angles

Nomenclature. Owing to the pronounced pseudosymmetry of mitridatite, it is convenient to arrange the polyhedral bond distances and bond length–bond strength variations according to structurally similar regions. The apical oxygens on PO_4 groups are indexed sequentially: for P(n) it is O($4n - 3$), n

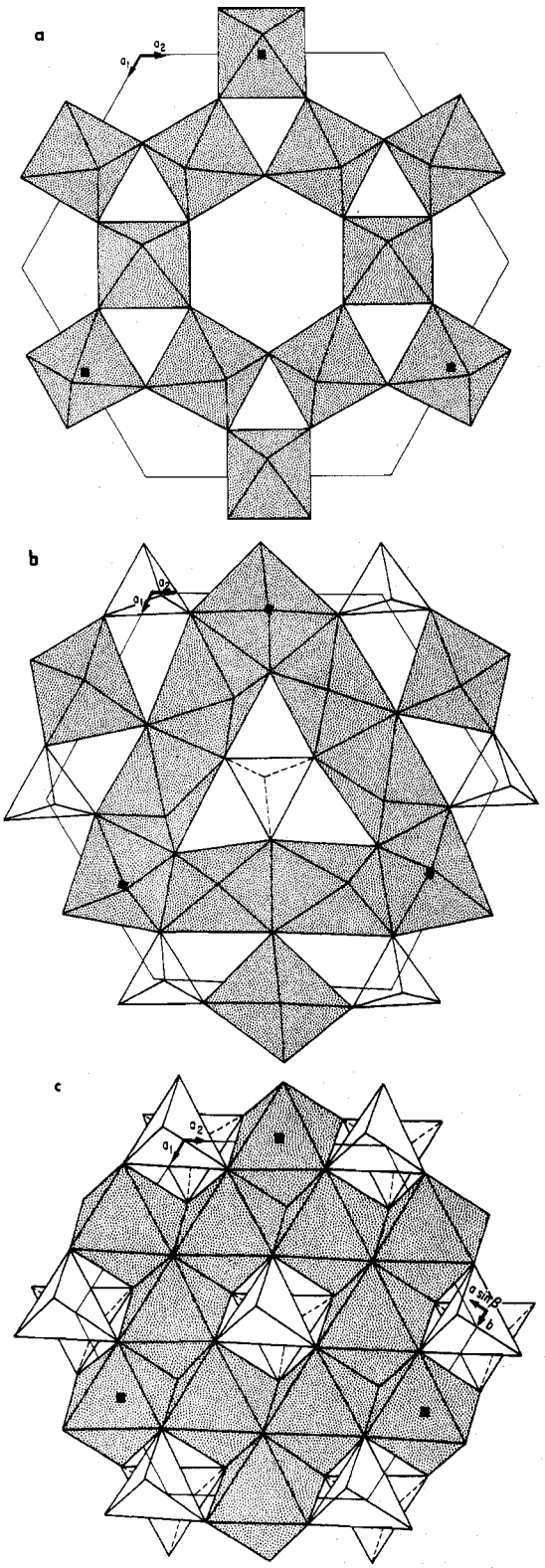

Figure 3. Sequence of progressively condensed octahedral sheets in (a) the alunite structure type, (b) mitridatite, and (c) hypothetical $[Fe^{III}_9O_6(PO_4)_6]^{3-}$. For orientation, refer to the three solid squares on each diagram.

= 1–9. The oxo anions are O(37)–O(42). There are two kinds of Fe atoms: three at the extreme pseudotrigonal corners (Fe(1) through Fe(3)) and the remaining six which comprise the central girdle (Fe(4) through Fe(9)). For true trigonal $p31m$ symmetry the atoms within the groupings would be equivalent. The first six P atoms, P(1) through P(6), are also related to each other by pseudosymmetry, and P(7) through P(9) are in geometrically similar environments. Finally, all six nonequivalent calcium atoms, Ca(1) through Ca(6), are related to each other in a pseudosymmetrical way. Thus, in Table III, the Fe–O, P–O, and Ca–O distances are arranged consistently, grouped according to the distinct kinds of oxygens. The O–O′ edge distances, however, are arranged in order of increasing distances following the more conventional procedure since we want to assess shared edge effects on these distances.

Ten kinds of oxygens are discerned and the first five are labeled in Figure 7. O_a and O_b are closely related and each is bonded to three Fe and one Ca. The O_a's are distributed at the triangular corners inside the nonamer and O_b's are the links between nonamers. The O_c oxygens correspond to the base of P(7) inside the nonamer and O_d are the bases of P(8) and P(9). Each of these bonds to two Fe and one P atom. The O_e oxygens are the bases of P(1) through P(6), akin to the alunite structure type, and link to Fe as termini above and below the sheets. They receive one bond from Fe, one from P, and one from Ca. The O_f's correspond to the apical oxygens of P(7) through P(9) and receive two hydrogen bonds (H_a) and one P bond. O_g are the apical oxygens of P(1) through P(6), similar to those found in the alunite structure type. There are two kinds: O_g receives one Ca and one P bond and O_g' receives an additional hydrogen bond from OW(7) through OW(9). The O_h's are OW(1) through OW(6) and each receives two Ca bonds and provides two hydrogen atom donors (H_d). Finally, O_i corresponds to OW(7) through OW(9) and each receives two hydrogen bonds (H_a) and donates two hydrogen bonds (H_d). One of the latter points to the base of P(7) through P(9) and is a weak bond: all O–H···O bonds are longer than 3.2 Å to any oxygen.

Figures 1, 4, and 5 afford the labeling of atoms; those unprimed indexes refer to the atomic positions in Table II, the primed indexes corresponding to positions generated by point set equivalence.

Assessment of Bond Length–Bond Strength Variations. Baur[20] has discussed the empirical relationships between bond length (d) and bond strength (s) for ionic inorganic crystals. For mineral structures, it is expected that the sum of bond strengths of cations about an anion, p_x, varies only slightly from the formal charge of that anion with reversed sign. Deviations (Δp_x) of a considerable degree should correlate with corresponding deviations in individual bond distance (Δd) with respect to the polyhedral average. The bond strength is evaluated $s = z/N_c$, where z is the formal charge of the cation and N_c is the coordination number of that cation. Therefore, $p_x = \sum_i s_i$ for the i cations surrounding (coordinated to) the anion. For hydrogen bonds, the hydrogen atom donor (H_d) bond is given $s = {}^5/_6$ and a hydrogen atom acceptor (H_a) bond $s = {}^1/_6$, suggested on empirical grounds by Baur.[20] Finally, Baur's fourth rule is invoked: "The lengths of the hydrogen bonds formed between pairs of anions vary inversely with Δp, the difference of the p_x-values received by the donor and acceptor atoms of the hydrogen bond: $\Delta p = p_{donor} - p_{acceptor}$."

Bond length–bond strength variations are important in assessing the role of water. In Table IV, the Δd and Δp_O are arranged according to the kind of oxygen. If more than one cation of a given kind coordinates to an anion the distance deviations were averaged. Inspection immediately shows that no hydroxyl (OH^-) anions occur in the structure; O_a, O_b, O_f, O_g, and O_g' treated as O^{2-} are all undersaturated ($\Delta p_O = -0.21$ to -0.46) and the individual distances are all considerably shorter than average. The reverse would be true if OH^- anions were present. O_c and O_d are considerably oversaturated ($\Delta p_O = +0.25$) and, consequently, the bond distances are longer than average. The agreement in distance deviations predicted from Baur's results of regression analyses[20] is quite acceptable. The O_e oxygens are nearly neutral ($\Delta p_O = +0.04$); deviations in

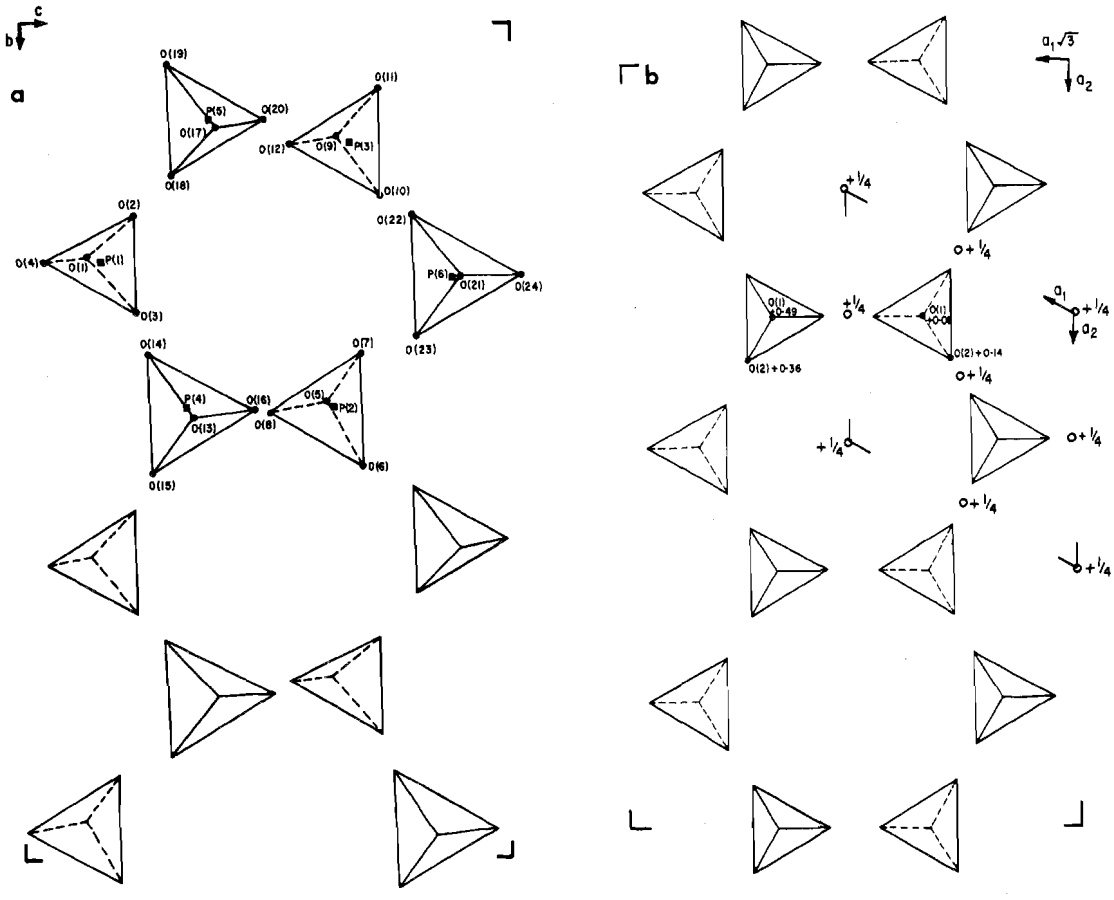

Figure 4. The $P(c)O_4$ tetrahedral isomorphisms between (a) mitridatite and (b) crandallite. The tetrahedra in (a) are those above and below $x = {}^1/_4$ and adopt the atom labels according to Table II. The tetrahedra in (b) were drawn from atom coordinates[8] which were inverted and translated $+{}^3/_4$ on z to facilitate comparison with (a). The crandallite cell is outlined and the inversion centers are drawn as open circles.

Δd are generally smaller than found for the more undersaturated and oversaturated oxygens. When the individual deviations are substantial for one cation (inspect O(6) and O(10)) they are compensated by the others. This analysis is extended to the water molecules of the type O_h and O_i. Here it is noted that $O_h \rightarrow O_f$ type bonds are all longer than predicted by Baur's regression analysis;[20] these are balanced by the $Ca-O_h$ bonds which are all shorter than predicted.

Since there are no contradictions, an unambiguous formula can be written for mitridatite. O_a and O_b must be accepted as oxo anions (O^{2-}) and there are no "acid" phosphate groups, hence the asymmetric unit is $Ca_6(H_2O)_6[Fe^{III}{}_9O_6(PO_4)_9]\cdot 3H_2O$ with the three water molecules after the period participating in hydrogen bonding only.

Bond Distances and Angles. Both bond strength sum deviations from local electrostatic neutrality and shared polyhedral edges account for patterns in individual bond distance deviations from polyhedral averages. $P-O_g$, O_g' range from 1.49 to 1.51 Å, about 0.03 to 0.05 Å shorter than their polyhedral averages. $Ca-O_g$, O_g' are also considerably foreshortened, ranging from 0.12 to 0.22 Å below the averages. These are well-understood from the principles discussed above.

Owing to cation–cation repulsions across shared edges, O–O′ distances associated with these edges are considerably foreshortened. Thus, in Table III, all such edges are the shortest for their polyhedra. The effect is most pronounced for the Fe–Fe′ cation pairs, but is clearly evident for Fe–Ca and Ca–Ca pairs as well. The Ca atoms are arranged above and below the O_a and O_b oxygens and the $CaO_5(H_2O)_2$ polyhedra share three of their edges with the FeO_6 octahedra. These edges are identified as those which emanate from the seventh coordinating oxygen (O_a or O_b) which lies above the octahedral face (Figure 6). It is noted that the octahedral face below the oxygen has edges which are the longest for the $CaO_5(H_2O)_2$ polyhedra. This clearly arises from the strain induced by the $^2_\infty[Fe_9O_{33}]$ octahedral sheets above and below owing to the rigid capping $P(c)O_4$ tetrahedra.

The nonamer itself is severely strained since it is a trigonal edge-sharing ring built of octahedra. Thus, the angles Fe(5)–Fe(1)–Fe(6) = 67.6 (1)°, Fe(4)–Fe(2)–Fe(9) = 67.8 (1)°, and Fe(7)–Fe(3)–Fe(8) = 69.1 (1)° are highly acute; for perfect octahedra these would each be 90°. Geometrically, it is impossible to construct the $^2_\infty[Fe_9O_{33}]$ sheet from octahedra and for this reason mitridatite is an unusual case of a complex oxide arrangement where distorted octahedra are implicit in its structure topology and geometry.

Isotypes and Derivative Structures

Two isotypes of mitridatite are known, arseniosiderite and robertsite, and their structure cell data are summarized in Table V. Arseniosiderite obtains from isomorphic replacement of (PO_4) by (AsO_4), resulting in slightly larger cell parameters. The most pronounced dilation is along the a direction since the contribution in this direction by the larger (AsO_4) tetrahedra is not constrained by the relatively rigid $^2_\infty[Fe_9O_{33}]$ sheets. Robertsite is particularly interesting since it is the $^2_\infty[Mn^{III}{}_9O_{33}]$ analogue of mitridatite and we anticipate a pronounced Jahn–Teller distortion of the octahedra owing to high spin $Mn^{3+}(3d^4)$ in an octahedral oxide field. Assuming that the distortion leads to apically elongated tetragonal bipyramidal coordination, we now predict the direction of distortion in the crystal structure. In studies on pinakiolite[21] $(Mg_2Mn^{III}O_2(BO_3))$, braunite[22] $(Mn^{II}Mn^{III}{}_6SiO_{12})$, and bermanite[17] $(Mn^{II}(H_2O)_4[Mn^{III}{}_2(OH)_2(PO_4)_2])$, it was noted that averages of four equatorial $Mn^{3+}-O^{2-}$ bonds range from 1.92 to 1.96 Å and the two apical $Mn^{3+}-O^{2-}$ bonds range from

Table IV. Mitridatite Correlations in Δp_O and Δd[a]

O_a $\Delta p_O = -0.21$ esu

	3Fe	Ca
37	−0.08	−0.03
40	−0.09	−0.05
41	−0.09	−0.01
p	−0.05	−0.07

O_b $\Delta p_O = -0.21$

	3Fe	Ca
38	−0.06	+0.01
39	−0.06	+0.00
42	−0.05	−0.02
p	−0.05	−0.07

O_c $\Delta p_O = +0.25$

	2Fe	P
26	+0.06	+0.02
27	+0.06	+0.01
28	+0.06	+0.03
p	+0.06	+0.03

O_d $\Delta p_O = +0.25$

	2Fe	P
30	+0.10	+0.01
31	+0.09	+0.00
32	+0.08	+0.03
34	+0.09	+0.02
35	+0.09	+0.02
36	+0.08	+0.00
p	+0.06	+0.03

O_h $\Delta p_O = +0.24$

	Ca	Hd
OW(1)	−0.02	
OW(2)	−0.02	
OW(3)	−0.04	
OW(4)	−0.02	
OW(5)	−0.03	
OW(6)	+0.00	
p	+0.08	

O_e $\Delta p_O = +0.04$

	Fe	Ca	P
2	−0.05	−0.07	+0.02
3	−0.03	+0.12	+0.01
4	−0.03	−0.03	+0.02
6	−0.05	+0.20	+0.01
7	+0.00	−0.05	+0.00
8	−0.04	−0.03	+0.01
10	−0.07	+0.34	+0.02
11	+0.00	+0.11	+0.00
12	−0.04	+0.18	+0.02
14	+0.02	+0.02	+0.02
15	−0.01	+0.33	−0.01
16	+0.04	−0.08	+0.01
18	−0.01	+0.06	+0.02
19	+0.01	−0.12	+0.02
20	+0.02	−0.08	+0.01
22	+0.02	−0.09	+0.01
23	−0.03	+0.43	+0.00
24	+0.02	+0.06	+0.01
p	0.00	+0.01	0.00

O_f $\Delta p_O = -0.42$

	2Ha	P
25		−0.06
29		−0.04
33		−0.04
p		−0.05

O_g $\Delta p_O = -0.46$

	Ca	P
1	−0.17	−0.05
5	−0.21	−0.04
17	−0.20	−0.06
p	−0.15	−0.05

O_g' $\Delta p_O = -0.30$

	Ca	Ha	P
9	−0.12		−0.06
13	−0.13		−0.04
21	−0.17		−0.03
p	−0.10		−0.04

[a] The columns are headed with designations for the oxygens, followed by bond distance deviations from polyhedral averages (Δd). The "p" refers to predicted values from regression analyses.[20]

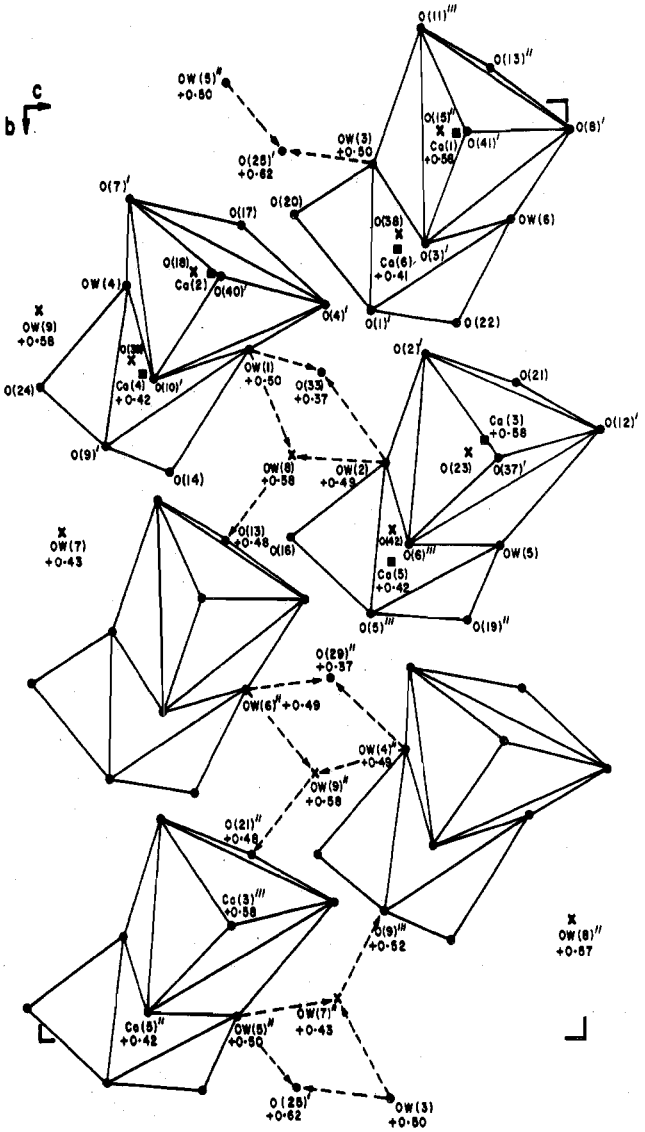

Figure 5. The open sheet of $CaO_5(H_2O)_2$ polyhedra and water molecules above and below the $x = {}^1/_2$ level. Heights are given as fractional coordinates in x. Note the occurrence of $Ca_2O_{10}(H_2O)_2$ dimers. Hydrogen bonds are drawn as dashed lines. Atoms are labeled according to Tables II and III.

2.23 to 2.26 Å. Depending on the degree of distortion Mn^{3+}–O polyhedral averages from 1.99 to 2.04 Å are obtained,[23] i.e., distance averages which are practically the same as those for Fe^{3+}–O. An hypothesis was advanced[17] that to best achieve local electrostatic neutrality, the apical Mn^{3+}–O bonds will be associated with oversaturated oxygens and the equatorial bonds with undersaturated oxygens. These scientists suggested as empirical bond strengths $s = {}^2/_6$ for apical bonds and $s = {}^{3.5}/_6$ for equatorial bonds. This means that O_c and O_d are apical oxygens, and O_a, O_b, and O_e are equatorial oxygens in robertsite. Note that $\Delta p_O = +0.035$ for O_a and O_b, −0.084 for O_c and O_d, and +0.119 for O_e, a marked improvement in approach to local electrostatic neutrality over the spherically symmetric distribution of bond strengths about the Fe^{3+}–O_6 octahedra in the mitridatite structure type. Geometrically, the isomorphic replacement of Fe^{3+} by Mn^{3+} in the mitridatite structure type would lead to a uniform dilation in the *bc* plane (average of two equatorial and two apical bonds about a ring) and a contraction of the *a*-axial direction (two equatorial bonds only). This is exactly what is observed in the cell parameter relations between robertsite and mitridatite. It is now evident why this kind of isomorphism exists for the mitridatite structure type: the distribution of undersaturated and oversaturated oxygens about octahedral M^{3+} cations is such that elongate tetragonal bipyramidal distortion leads to smaller deviations from local electrostatic neutrality.

Table V. Crystal-Chemical Relationships between Mitridatite and Related Phases[a]

Species	a, Å	b, Å	c, Å	β, deg	Formula
Mitridatite	17.52	19.35	11.25	95.92	$Ca_6(H_2O)_6[Fe^{III}{}_3Fe^{III}{}_6O_6(PO_4)(PO_4)_2(PO_4)_6]\cdot 3H_2O$
Robertsite	17.36	19.53	11.30	96.0	$Ca_6(H_2O)_6[Mn^{III}{}_3Mn^{III}{}_6O_6(PO_4)(PO_4)_2(PO_4)_6]\cdot 3H_2O$
Arseniosiderite	17.76	19.53	11.30	96.0	$Ca_6(H_2O)_6[Fe^{III}{}_3Fe^{III}{}_6O_6(AsO_4)(AsO_4)_2(AsO_4)_6]\cdot 3H_2O$
Betpakdalite	17.73	19.25	11.22	92.5	$Ca(H_2O)_2[\square_3Mo^{VI}{}_5Fe^{III}O_6(FeO_4)(AsO_4)_2(OH)_{12}]\cdot 6H_2O$
Melkovite	17.46	18.48	10.93	94.5	$Ca(H_2O)_2[\square_3Mo^{VI}{}_5Fe^{III}O_6(FeO_4)(PO_4)_2(OH)_{12}]\cdot 6H_2O$

[a] The cell parameters for the first three compounds are quoted from ref 4 and the last two from ref 23.

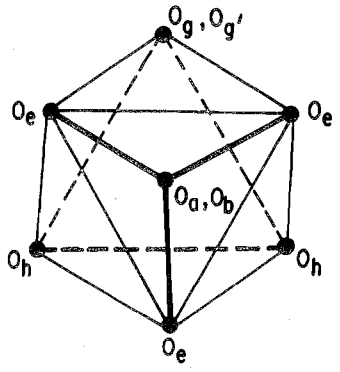

Figure 6. Labeling of the $CaO_5(H_2O)_2$ oxygens according to their type. Shared edges on the polyhedron, here shown idealized, are drawn bold.

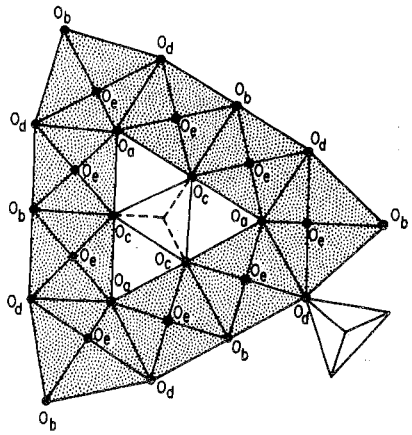

Figure 7. Labeling of the oxygens O_a through O_e about the idealized octahedral nonameric ring.

Table V also lists two compounds, betpakdalite and melkovite, which we suspect are derivative structures of the mitridatite structure type. Their morphological characters and reported structure cell parameters[23] reveal a close relationship to mitridatite. The authors proposed $CaFe^{III}_2(H_2O)_{14}[As_2Mo_5O_{24}]$ for betpakdalite; we suggest it be isomorphically rearranged into a mitridatite formula, that is $Ca(H_2O)_5[\square_3(Mo^{VI}_5Fe^{III})O_6(FeO_4)(AsO_4)_2(OH)_{12}]\cdot 3H_2O$. Here, the three Fe(a) atoms in mitridatite are voided (=□) and the P(c)O_4 tetrahedra are voided, the free octahedral apices above and below bonded to $(OH)^-$ groups only. Note that local electrostatic neutrality is well-preserved in this model, with Δp_{O_a}, $\Delta p_{O_b} \sim 0.00$, $\Delta p_{O_c} \sim +0.75$, $\Delta p_{O_d} \sim +0.25$, and $\Delta p_{O_e} \sim 0.00$. The structure, in effect, is a linkage of central girdles of the Keggin molecule by tetrahedra; the girdle and central tetrahedron have average composition $[^{[6]}(Mo_5Fe)^{[4]}Fe\text{-}O_{16}(OH)_{12}]$.

Acknowledgment. It is a pleasure to thank the National Science Foundation whose support through Grant GA-40543 awarded to P.B.M. and a Materials Research Laboratory grant awarded to The University of Chicago made possible the collection of samples and the completion of the structure investigation.

Registry No. Mitridatite, $Ca_6(H_2O)_6[Fe^{III}_9O_6(PO_4)_9]\cdot 3H_2O$, 61966-51-6.

Supplementary Material Available: Listing of structure factor amplitudes (46 pages). Ordering information can be found on any current masthead page.

References and Notes

(1) S. P. Popov, *Tr. Geol. Muzeya Akad. Nauk*, **7** (1910).
(2) F. V. Chukhrov, *Tr. Lomonosovsk. Inst. Geokhim., Kristallogr. Mineral., Akad. Nauk SSSR*, **10** (1937).
(3) A. V. Sidorenko, *Dokl. Akad. Nauk SSSR*, **48**, xx (1945).
(4) P. B. Moore, *Am. Mineral.*, **59**, 48 (1974).
(5) P. B. Moore and T. Araki, *Mineral. Mag.*, in press.
(6) C. W. Burnham, *Am. Mineral.*, **51**, 159 (1966).
(7) P. B. Moore and T. Araki, *Inorg. Chem.*, **15**, 316 (1976).
(8) A. M. Blount, *Am. Mineral.*, **59**, 41 (1974).
(9) G. N. Ramachandran and R. Srinivasan, "Fourier Methods in Crystallography", Wiley-Interscience, New York, N.Y., 1970, p 96.
(10) W. H. Zachariasen, *Acta Crystallogr., Sect. A*, **24**, 425 (1968).
(11) D. T. Cromer and J. B. Mann, *Acta Crystallogr., Sect. A*, **24**, 321 (1968).
(12) D. T. Cromer and D. Liberman, Report LA-4403, UC-34, Los Alamos Scientific Laboratory, University of California, Berkeley, Calif., 1970.
(13) H. D'Amour, *Acta Crystallogr., Sect. B*, **32**, 729 (1976).
(14) L. Fanfani, A. Nunzi, P. F. Zanazzi, A. R. Zanzari, and C. Sabelli, *Mineral. Mag.*, **40**, 131 (1975).
(15) R. Wang, W. F. Bradley, and H. Steinfink, *Acta Crystallogr.*, **18**, 249 (1965).
(16) K. H. Wedepohl, Ed., "Handbook of Geochemistry", Vol. II, Part 3. Springer-Verlag, Berlin, 1972, p 13-A-1.
(17) A. R. Kampf and P. B. Moore, *Am. Mineral.*, **61**, 1241 (1976).
(18) P. B. Moore, *Mineral. Mag.*, **40**, 863 (1976).
(19) G. R. Rossman, *Am. Mineral.*, **61**, 398 (1976).
(20) W. H. Baur, *Trans. Am. Crystallogr. Assoc.*, **6**, 129 (1970).
(21) P. B. Moore and T. Araki, *Am. Mineral.*, **59**, 985 (1974).
(22) R. D. Shannon, P. S. Gumerman, and J. Chenavas, *Am. Mineral.*, **60**, 714 (1975).
(23) K. V. Skvortsova, G. A. Sidorenko, Yu. S. Nesterova, G. A. Arapova, A. D. Dara, and L. I. Rybakova, *Int. Geol. Rev.*, **14**, 473 (1972).